J. Fluid Mech. (1985), *vol.* 151, *pp.* 81–103
Printed in Great Britain

On the fine-scale intermittency of turbulence

By K. R. SREENIVASAN
Applied Mechanics, Mason Laboratory, Yale University

(Received 23 September 1983 and in revised form 15 May 1984)

This paper presents a simple theory for evaluating the several measures used to characterize the intermittency of fine-scale turbulence, and corroborates the theoretical results from comparison with experimental data, some of which are new. The basic analytical tool is the envelope of the narrow-bandpass-filtered turbulent signal, defined via its Hilbert transform and the analytic signal. The contribution of this paper is twofold. First, it correctly identifies the roles played by the filter characteristics (such as the bandwidth) in determining the intermittency factor, the width of the active regions (pulses) in narrow-bandpass-filtered turbulent signals, and the pulse frequency; it also reveals that all dynamical characteristics of the signal enter indirectly through the peak pulse frequency and the threshold setting. Secondly, the theory suggests that, in the far-dissipation range, the most important feature of signals exhibiting internal intermittency is the stronger-than-algebraic roll-off of the spectral density in that region; it is argued that this feature of turbulence essentially determines the peak pulse frequency in that region. The theory is incomplete in that it does not show how the threshold setting depends on the signal dynamics, but here the discussion is supplemented by experimental data.

1. Introduction

In a seminal paper, Batchelor & Townsend (1949) made the discovery that the fine structure of turbulence in high-Reynolds-number flows is both spatially and temporally intermittent. The experimental evidence at the time consisted of successively differentiated velocity signals which showed an increasingly 'binary' character with narrow regions of high activity separated by those of relative quiescence. Batchelor & Townsend's measurements were confined to grid turbulence and wakes, but the subsequent experimental work – to name just a few – of Sandborn (1959) in turbulent boundary layers, of Kennedy & Corrsin (1961) in the free shear layer at the exit of a square duct, of Grant, Stewart & Moilliet (1962) in a tidal channel, of Badri Narayanan, Narasimha & Rao (1971) in a fully developed duct flow, Kuo & Corrsin (1971) in far-field jets, etc., has established that the fine-scale intermittency, or 'spottiness', is a common occurrence in turbulence, and one of its important attributes.

The recognition of the basic nature of fine-scale (or 'internal') intermittency has led to a profound change in our understanding of small-scale turbulence. It has led to a modification in a very vital way of the 'universal similarity hypothesis' of Kolmogorov (1941) according to which energy cascade down the wavenumber spectrum occurs at high Reynolds numbers in such a way that all statistical information, except for the mean energy-dissipation rate itself, is lost on the 'universal, isotropic and homogeneously distributed' small scales of motion.

A lot of work on fine-scale intermittency has occurred, principally in three different, albeit interacting, directions. The first of them is a group of arguments that

can be designated collectively as the scale-similarity arguments. The second variety, which does not recognize the energy cascade explicitly, leads to 'mechanistic' models of fine structure. The third, of course, is the experimental work in turbulent flows. Each of these groups deserves to be commented on briefly.

The scale-similarity arguments go essentially thus. Within a given field of turbulence, consider a cube with sides of length L_0, where L_0 is an integral scale of turbulence. If we divide this cube into an arbitrarily large number $n(\gg 1)$ of smaller cubes of length $L_1 = L_0 n^{-\frac{1}{3}}$, the simplest picture of internal intermittency implies that the fine-scale turbulence is not uniformly distributed over all the cubes of linear dimension L_1 but only over some of them. Novikov & Stewart (1964) proposed a rather specific model which envisaged that practically all the dissipative fine structure exists in only a few of these first-order cubes (say m of them, $m \ll n$) distributed in a random fashion. Further subdivision of these cubes into second-order ones of length $L_2 = L_1 n^{-\frac{1}{3}}$, it is hypothesized, would show that the dissipation is contained only in some small number of these second-order cubes, and so on. This is also the so-called absolute curdling of Mandelbrot (1976). Instead of assuming that some subcubes contain all the dissipation and some nothing, if one assumes, for a fixed dissipation rate in a cube of order j, that the density of dissipation rate in each subcube of order $j+1$ is multiplied by a random variable g, with $\langle g \rangle = 1$, then the so-called 'weighted curdling' of Mandelbrot, or the 'cascade process of eddy breakdown' of Yaglom (1966) results. The essence of the argument here is that the probability density function g is assumed to be independent of j until one reaches sizes where viscous effect becomes directly important. If $\log g$ is assumed to be normally distributed, one obtains the famous lognormal distribution proposed by Kolmogorov (1962). It should be emphasized – as has been done on several occasions, for example, by Kraichnan (1974), Mandelbrot (1976), Frisch, Sulem & Nelkin (1978) – that the lognormal model is only one of several possibilities with no special merit to it, and that the large measure of past preoccupation with it is probably unwarranted. It is to be noted that none of the models discussed in this paragraph makes a direct appeal to the Navier–Stokes equations.

The motivating factor for the second group of models appears to be the vortex-stretching phenomenon; there is thus an implied connection here with the Navier–Stokes equations. The earliest model is perhaps due to Townsend (1951), who, however, did not incorporate spottiness explicitly. Several years later, Corrsin (1962) visualized a model in which the fine structure was made up of vortex sheets of thickness of the order of Kolmogorov's microscale η, with a mean separation distance of the order of an integral scale of turbulence. Tennekes (1968) pointed out that the model is inconsistent because it predicts an incorrect order of magnitude for the energy-dissipation rate, and proposed an alternative model in which the vortex concentration occurs in the form of tubes (rather than sheets) with diameters of the order of η and spacing of the order of the Taylor microscale λ. Neither of these models predicts the correct dependence of skewness and flatness factors on the Reynolds number (e.g. Van Atta & Antonia 1980), and so must be considered incomplete if not incorrect. (We may also note that Mandelbrot (1976) dismisses these models as incorect; his reasoning is related to fractal dimensions and will not be repeated here.) Saffman (1968) assumed that vorticity is concentrated in the form of tubes and sheets with the characteristic dimension of the order of $\delta \equiv (\nu/\alpha)^{\frac{1}{2}}$, where α is the local straining rate. If the concentration of vorticity is assumed to occur by the straining due to large eddies, it follows that $\alpha = \tilde{u}/L_0$, where $\tilde{u}$ is a characteristic velocity of the large eddies. However, in contrast with experimental findings (see e.g. Sreenivasan

1984), the model predicts a dissipation rate that is strongly Reynolds-number dependent. To avoid this inconsistency, Saffman further hypothesized that the vortex sheets and tubes undergo a secondary instability of the Taylor–Görtler type; this results in the concentration of vorticity effectively into thin sheets of thickness of the order of η, and spacing of the order of δ. (At this point, it is worth pointing out that the fine structure is as often identified with vorticity as with dissipative eddies. However, regions of strong dissipation do not always coincide with regions of strong vorticity (see, for example, the direct numerical solution of the Navier–Stokes equations for the Taylor–Green flow by Brachet *et al.* 1983). Consequently, it is possible that slightly different conclusions may arise depending on whether one means by fine structure dissipative eddies or vorticity-bearing ones. This is not the only source of ambiguity in the literature on fine-scale turbulence. Experimentally, one measures most often the characteristics of the rate of strain $\partial u/\partial x$ – again, regions of strong $\partial u/\partial x$ do not coincide with regions of strong vorticity (see Siggia 1981) – which itself is obtained by invoking Taylor's frozen-field approximation; here u is the velocity fluctuation in the longitudinal (or mainstream) direction x. Alternatively, one also examines the output of narrow-bandpass filters or high-pass filters set appropriately high. In spite of these ambiguities, one *hopes* that the main attributes of internal intermittency somehow come through.)

The earliest experimental studies are due to Batchelor & Townsend (1949) who estimated the internal intermittency factor from measurements of the flatness factors of differentiated or bandpass-filtered velocity signals. The justification for this procedure was simply that for an ideally intermittent on–off signal which has a flatness factor F_0 for its 'on part', the intermittency factor γ is related to the overall flatness factor F by the relation

$$F = F_0/\gamma. \tag{1.1}$$

If the 'on part' is Gaussian, $F_0 = 3$. In practice, the 'off part' is not completely quiescent, nor is the 'on part' Gaussian, and so the intermittency factor can be inferred from flatness-factor measurements only if the probability distributions of both states are known. Kennedy & Corrsin (1961) emphasized this, and also showed that larger derivative flatness does not necessarily imply larger intermittency. Following this rationale, direct measurements of the intermittency factor have later been made by Kuo & Corrsin (1971), who also obtained information about the linear dimension, or 'width', of these fine-scale regions. Further information about the fine structure was obtained by Kuo & Corrsin (1972), who attempted to determine the geometry of the fine-scale regions by measuring the dependence of the two-probe intermittency on the spatial separation of the probes. Briefly, their conclusions appear to suggest a greater tendency of the fine structure to be filament-like in its geometry rather than blob-like or sheet-like.

The work of Rao, Narasimha & Badri Narayanan (1971) is also of interest here. Rao *et al.* systematically examined turbulent velocity signals by bandpass filtering them at various mid-band frequencies. Their contribution was in devising a method for counting at high Reynolds numbers (where visual counting becomes very difficult) the frequency of active regions in narrow-bandpassed signals – the so-called pulses in the terminology of Badri Narayanan, Rajagopalan & Narasimha (1977) – and in concluding that the mean spatial separation distance between the pulses is of the order of the integral scale of turbulence – a result which was qualitatively anticipated by Batchelor & Townsend (1949). Badri Narayanan *et al.* (1971) extended these measurements to other shear flows and arrived at similar conclusions, although their

measurements in grid turbulence were inconclusive. More detailed measurements of similar type have also been made by Badri Narayanan, Rajagopalan & Narasimha (1974, 1977) and Antonia, Danh & Prabhu (1976). These authors also obtained information on the width of the pulses.

Unfortunately, an examination of these various recent data shows large differences – real or apparent, qualitative and quantitative – among them. For instance, in the measurements of Rao *et al.* and Badri Narayanan *et al.* the mean frequency of the occurrence of active regions has tended to be independent of the mid-frequency setting of the bandpass filter beyond a certain setting; on the other hand, Antonia *et al.* did not find a conclusive asymptote, but only a break point above which the rate of increase of frequency became smaller. Kuo & Corrsin's measurements, however, showed that the pulse frequency initially increased as the filter setting was increased and then decreased. The normalized estimates of the mean spacing between the pulses determined by the various authors differ among themselves by a factor of about 10. Further, the fine-scale intermittency factor γ as well as the (normalized) pulse width were found to be independent of Reynolds number by Antonia *et al.*, whereas Kuo & Corrsin's measurements showed a decrease at low Reynolds numbers before settling down to a constant beyond a microscale Reynolds number of 350; this constant, however, was numerically different from the value found by Antonia *et al.* Badri Narayanan *et al.* found both γ and the pulse width to increase monotonically with Reynolds number.

Evidently either these different authors were measuring different parameters without explicitly recognizing it to be so, or that extraneous effects distorted the results in one or the other (or all) of them. An assessment of the various experimental techniques used in these recent experiments, with a view to consolidating the genuine common ground as well as isolating points of departure among them, is a major motivation for this paper. In the course of the work that followed, it became clear that some of the properties attributed to fine-scale turbulence are also shared by other bandpass-filtered random processes; at any rate, it did not seem necessary to invoke explicitly any special dynamical features for explaining some of those observations. Filter characteristics were also determined to be extremely important. To put these preliminary conclusions on firmer ground, we undertook to examine a simple analytical tool with a fairly wide applicability in the study of random signals passed through narrow-band filters. Corroborating measurements were also made. The net picture that emerges is fairly simple, and seems to explain rather well most observations and remove nearly all the discrepancies which seemed to prevail at a first look.

In §§2 and 3 a description of the analytical method is given, and its performance is assessed for comparison with the new test-case experiments with an essentially Gaussian process. In §4 measurements (some of which are new) relating to turbulent signals in boundary layers and flow behind grids are examined in the light of the results derived in §§2 and 3. Section 5 contains a summary of conclusions which also assesses the significance of this work.

2. Analytical preliminaries

2.1. *Motivation*

For identifying the high-frequency pulses and determining their statistical properties, Badri Narayanan *et al.* (1977) described and used a signal-processing technique. This technique, also used by Antonia *et al.* (1976), differs from that of Rao *et al.* (1971)

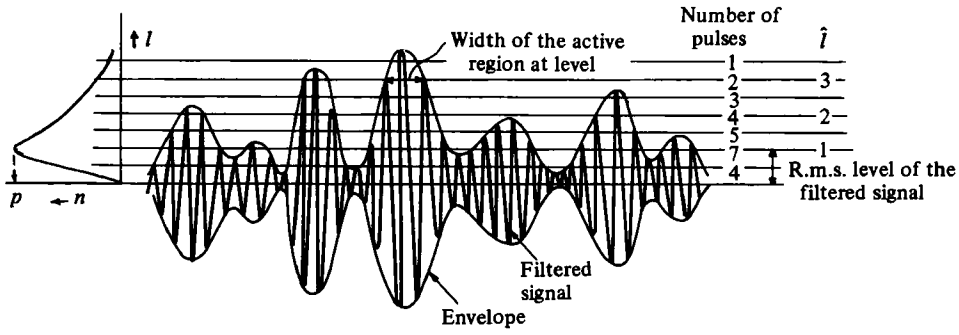

FIGURE 1. A schematic of a turbulent signal bandpass-filtered at some midband frequency f_m. The crossing frequency $\hat{n}$ as a function of the level $\hat{l}$ (that is, the distance from the zero of the filtered signal normalized by its own root-mean-square value) is indicated on the left. $\hat{n}_p$ is the maximum of $\hat{n}(\hat{l})$.

only in some detail, and bears a close relation to that used by Kuo & Corrsin (1971). A brief description of this technique will therefore serve as a useful and necessary starting point.

In this technique, a given turbulent signal is filtered through a bandpass filter at a mid-frequency f_m. This results in an amplitude-modulated signal of frequency f_m with the period of modulation corresponding to the inverse of the filter bandwidth (see figure 1). Regions of activity in this bandpass-filtered signal are designated here (following Badri Narayanan *et al.* 1977) as pulses. An envelope is then drawn over the bandpassed signal and the positive crossing frequency $\hat{n}$ of the envelope is determined as a function of the threshold $\hat{l}$, say. Clearly, this frequency will have a peak for some $\hat{l}$; we denote the peak frequency in the $\hat{n}$ versus $\hat{l}$ curve by $\hat{n}_p$ (see figure 1). In general, $\hat{n}_p$ is a function of the selected midband frequency f_m. This exercise is therefore repeated for several values of f_m, and the variation of $\hat{n}_p$ with f_m is determined. For turbulent signals, the measurements of Rao *et al.* have shown that $\hat{n}_p$ increases with f_m when f_m is low (typically in the energy-containing frequency range), but asymptotically becomes independent of f_m when f_m is high (typically in the dissipation range) – a result that those authors attributed to fine-scale intermittency. In their further work, the asymptotic value of $\hat{n}_p$, say $\hat{N}_p$, corresponding to the essentially flat region of the $\hat{n}_p$ versus f_m curve, played an important role as the characteristic pulse frequency of the turbulent signal. Because the mechanics of this signal processing are fairly complicated, it seems appropriate to understand its details before attempting to interpret the results; this is essentially the motivation for the discussion in this and the next sections. Neither Rao *et al.* nor Badri Narayanan *et al.* offered any explanation for the behaviour of $\hat{n}$ versus $\hat{l}$ or $\hat{n}_p$ versus f_m curves.

2.2. *Theoretical background*

Let $x(t)$ be a stationary stochastic process with zero mean, continuous in the quadratic mean, defined as

$$x(t) = \int_{-\infty}^{\infty} e^{i\omega t}\, d\zeta(\omega). \tag{2.1}$$

Define the Hilbert transform $y(t)$ of $x(t)$ by

$$y(t) = -\int_{-\infty}^{\infty} i \operatorname{sgn}\omega\, e^{i\omega t}\, d\zeta(\omega), \tag{2.2}$$

where $\operatorname{sgn}\omega = \pm 1$ when $\omega \gtrless 0$. It is seen that taking Hilbert transform is equivalent to a curious kind of linear transformation in which the amplitude remains unchanged, but the phase gets shifted by $\pm\frac{1}{2}\pi$ depending on the sign of ω. By convolution theorem, it follows that

$$y(t) = -\frac{1}{\pi t} * x(t).$$

Form the complex function

$$z(t) = x(t) + \mathrm{i}\, y(t).$$

Now, $z(t)$ is called the analytic signal of $x(t)$. The significance of the analytic signal is known from communication theory; briefly, it bears the same relation to $x(t)$ as $\exp(\mathrm{i}t)$ does to $\cos t$. The original signal $x(t)$ can be recovered from the analytic signal $z(t)$ by projection on the real axis. For a somewhat elaborate discussion, see e.g. Bracewell (1965). The envelope $E(t)$ of $x(t)$ is then simply defined as the modulus of the analytic signal $z(t)$. That is,

$$E(t) = |z(t)| = [x^2(t) + y^2(t)]^{\frac{1}{2}}. \tag{2.3}$$

To see that this definition is meaningful, consider first some simple cases.

(i) Let $x(t) = A\cos(\omega_1 t + \theta_1)$, $\omega_1 > 0$, and form the complex function

$$z(t) = A\,\mathrm{e}^{\mathrm{i}(\omega_1 t + \theta_1)}$$

with its real part equal to $x(t)$. Clearly

$$|z(t)| = A$$

is the envelope $E(t)$ of $x(t)$. For the function $B\sin(\omega_2 t + \theta_2)$ it is easily shown that the corresponding analytic signal is $-\mathrm{i}B\,\mathrm{e}^{-\mathrm{i}(\omega_2 t + \theta_2)}$, and the same interpretation of the envelope holds.

(ii) Consider $x(t) = A\cos(\omega_1 t + \theta_1) + B\sin(\omega_2 t + \theta_2)$. The analytic signal is given as

$$z(t) = A\,\mathrm{e}^{\mathrm{i}(\omega_1 t + \theta_1)} - \mathrm{i}B\,\mathrm{e}^{\mathrm{i}(\omega_2 t + \theta_2)},$$

whose absolute value defines the envelope of $z(t)$.

It is not hard to visualize (by actually working out the details) that this is indeed a meaningful definition of the envelope when, say, $\omega_1 + \omega_2 \gg \omega_1 - \omega_2$.

(iii) Consider a more complicated function

$$x(t) = \sum_{n=0}^{\infty} A_n \cos\omega_n t + \sum_{n=0}^{\infty} B_n \sin\omega_n t.$$

By analogy with (ii) above,

$$z(t) = \sum_{n=0}^{\infty} A_n\,\mathrm{e}^{\mathrm{i}\omega_n t} - \mathrm{i}\sum_{n=0}^{\infty} B_n\,\mathrm{e}^{-\mathrm{i}\omega_n t}.$$

Again, the envelope is defined as $|z|$. While this is not easy to visualize physically, $|z|$ clearly satisfies the mathematical requirements of an envelope.

(iv) Finally, consider a real continuous stochastic process defined by (2.1), which can alternatively be written as

$$x(t) = \int_0^{\infty} (\mathrm{d}\lambda\cos\omega t + \mathrm{d}\eta\sin\omega t),$$

where $$\lambda(\omega) = \zeta(\omega) - \zeta(-\omega), \quad \eta(\omega) = \mathrm{i}(\zeta(\omega) + \zeta(-\omega)).$$

By analogy with (iii), we have

$$z(t) = x(t) + \mathrm{i}y(t),$$

where y is defined by (2.2). Again, $|z(t)|$ is defined as the envelope of $x(t)$. For a physically meaningful picture, it is necessary to restrict $x(t)$ to narrow-band signals, and, as we shall discuss more fully in §2.3, this is done here.

In particular, let $x(t)$ be a Gaussian process possessing finite first and second spectral moments m_1 and m_2 defined by

$$m_r = \int_0^\infty \omega^r \phi(\omega)\, \mathrm{d}\omega, \quad r = 1, 2. \tag{2.4}$$

Here, $\omega = 2\pi f$ is the angular frequency and $\phi(\omega)$ is the power-spectral density of $x(t)$ defined such that

$$\int_0^\infty \phi(\omega)\, \mathrm{d}\omega = m_0, \tag{2.5}$$

where m_0 is the mean-square value of $x(t)$. For these conditions, it has been shown (e.g. Cramer & Leadbetter 1967) that the expected number of positive crossings n of a level l (normalized by the root-mean-square value of $x(t)$) of $E(t)$ is given by the Rayleigh distribution

$$n(l) = (\xi/2\pi)^{\frac{1}{2}} l\, \mathrm{e}^{-\frac{1}{2}l^2}, \tag{2.6}$$

where† $$\xi = \frac{m_2}{m_0} - \left(\frac{m_1}{m_0}\right)^2. \tag{2.7}$$

The peak value of this distribution

$$n_\mathrm{p} = \max_l n(l) = n(1)$$

is given by $$n_\mathrm{p} = (\xi/2\pi\mathrm{e})^{\frac{1}{2}}. \tag{2.8}$$

Thus, all one needs to know to determine n_p for a given Gaussian process $x(t)$ are the first three moments m_0, m_1 and m_2 of its real spectral density $\phi(\omega)$. The crossing frequency at any level l follows from (2.6) and (2.8) to be

$$n(l)/n_\mathrm{p} = \mathrm{e}^{\frac{1}{2}} l\, \mathrm{e}^{-\frac{1}{2}l^2}. \tag{2.9}$$

At any given threshold level l, we can define the width of the active region as the interval between an upcrossing and a subsequent downcrossing of l by the envelope $E(t)$ (see figure 1). Then it can be shown (e.g. Cramer & Leadbetter 1967) that the mean width W_a of the active region (that is, the region above the threshold level) is given by

$$W_\mathrm{a}(l) = (2\pi/\xi l^2)^{\frac{1}{2}}. \tag{2.10}$$

Define now the fraction of the total time the signal is active (i.e. enclosed within the envelope) as the intermittency factor γ associated with the signal. Then it follows from (2.6) and (2.10) that

$$\gamma \equiv W_\mathrm{a}\, n = \mathrm{e}^{-\frac{1}{2}l^2}. \tag{2.11}$$

Note that the intermittency factor γ is independent of the form of the spectral density $\phi(\omega)$. Another convenient relation is

$$W_\mathrm{a}\, n_\mathrm{p}\, l = \mathrm{e}^{-\frac{1}{2}} \approx 0.607. \tag{2.12}$$

2.3. *Bandpass-filtered signals*

Although the envelope defined in §2.1 is of general mathematical validity, it is not necessarily always a well-defined physical entity for wide-band stochastic processes.

† Noting that $\phi(\omega) \geqslant 0$ for all ω, straightforward application of Schwarz's inequality shows that $\xi \geqslant 0$ always.

On the other hand, for narrow-bandpass-filtered random signals, it is a perfectly realizable entity (see figure 1); this is precisely why the envelope defined through the analytic signal becomes a useful tool in internal intermittency studies. Our concern is essentially with the narrow-bandpass-filtered signals, say $\hat{x}(t;\Delta;f_m)$, obtained by passing the signal $x(t)$ through a bandpass filter of constant *fractional* bandwidth Δ set to a midband frequency f_m. We can now treat the bandpass-filtered signal $\hat{x}$ as a new stochastic process, whose spectral density is the same (except for the scaling factor) as that of the original unfiltered signal $x(t)$ in the narrow bandwidth chosen, and zero everywhere else. It follows that the quantities corresponding to (2.3), (2.4), (2.7)–(2.9), (2.11) and (2.12) are

$$\hat{E}(t) = |\hat{z}(t)| = [\hat{x}^2(t)+\hat{y}^2(t)]^{\frac{1}{2}}, \tag{2.13}$$

$$\hat{m}_r = \int_{\omega_m(1-\frac{1}{2}\Delta)}^{\omega_m(1+\frac{1}{2}\Delta)} \omega^r \phi(\omega)\,\mathrm{d}\omega, \quad r = 0, 1, 2, \tag{2.14}$$

$$\hat{\xi} = \left(\frac{\hat{m}_2}{\hat{m}_0}\right) - \left(\frac{\hat{m}_1}{\hat{m}_0}\right)^2, \tag{2.15}$$

$$\hat{n}_p = (\hat{\xi}/2\pi\mathrm{e})^{\frac{1}{2}}, \tag{2.16}$$

$$\hat{n}(\hat{l})/\hat{n}_p = \hat{l}\exp[-\tfrac{1}{2}(\hat{l}^2-1)], \tag{2.17}$$

$$\gamma = \exp(-\tfrac{1}{2}\hat{l}^2), \tag{2.18}$$

$$\hat{W}_a\,\hat{n}_p\,\hat{l} = \mathrm{e}^{-\frac{1}{2}}. \tag{2.19}$$

Here $\phi(\omega)$ is the spectral density of the *unfiltered* signal $x(t)$ from which $\hat{x}(t)$ is derived from bandpass-filtering around the midband frequency $f_m = \omega_m/2\pi$; and $\hat{l}$ is the crossing level normalized by the root-mean-square of the bandpass-filtered signal $\hat{x}(t;\Delta;f_m)$. All the variables defined in (2.13)–(2.16) depend in general on both Δ and f_m, but this dependence will not always be explicitly mentioned. The symbol $\hat{}$ will, however, be used consistently to denote quantities associated with bandpass-filtered signals.

3. Results for bandpass-filtered random Gaussian processes

3.1. *White noise*

White noise, for which $\phi(\omega)$ = constant, is quite often adequately described by a Gaussian probability density function. When bandpass-filtered, the spectral density is ideally a constant within the bandwidth and zero everywhere else.† It follows from (2.14), (2.15) and (2.16) that

$$\frac{\hat{n}_p}{f_m\Delta} = \left(\frac{\pi}{6\mathrm{e}}\right)^{\frac{1}{2}} \approx 0.44. \tag{3.1}$$

From (2.19) and (3.1) we have

$$\hat{W}_a\,f_m\,\Delta\hat{l} = (6/\pi)^{\frac{1}{2}} \approx 1.38. \tag{3.2}$$

Finally

$$\gamma = \mathrm{e}^{-\frac{1}{2}\hat{l}^2}. \tag{3.3}$$

Equation (3.1) shows that, for a given bandwidth, the peak pulse frequency $\hat{n}_p$ increases linearly with the midband frequency and, for a given midband frequency,

† Since the filtering operation is linear, the probability density of the filtered signal is also Gaussian.

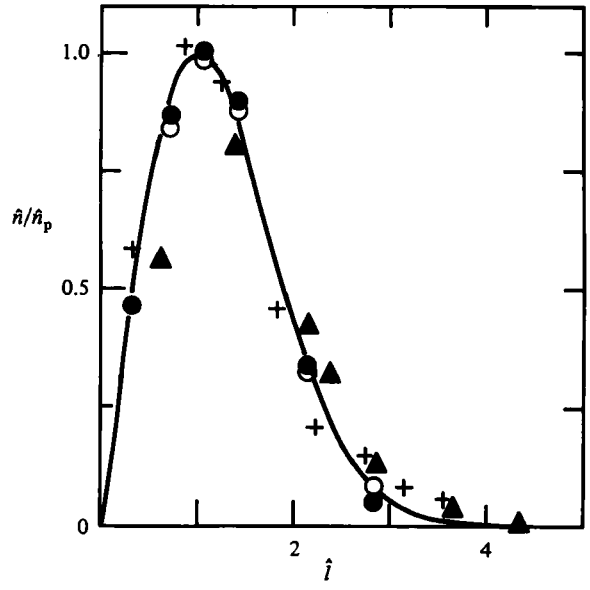

FIGURE 2. The pulse frequency $\hat{n}$ in filtered white-noise signals as a function of the level of crossing $\hat{l}$; the bandwidth $\Delta = 0.52$; +, $f_m = 500$ Hz, measured $\hat{n}_p = 110$ Hz; ○, ●, $f_m = 1000$ Hz, $\hat{n}_p = 208$ Hz (filled and unfilled circles correspond to either side of zero of the filtered signal); △, $f_m = 2500$ Hz, $\hat{n}_p = 585$ Hz; ——, equation (2.17).

increases linearly with the fractional bandwidth. It follows from (3.2) that, for fixed fractional bandwidth Δ and level $\hat{l}$, the width $\hat{W}_a$ of the active regions in the bandpassed signal is inversely proportional to the midband frequency. Interestingly, it is seen from (3.3) that γ is independent of f_m and the bandwidth Δ.

Before we attempt to confirm these results by experiment, it is necessary to establish the meaning of the parameter Δ used in (3.1) and (3.2). In this theory, Δ is the width of an ideal narrow-bandpass filter, which is assumed to have a perfectly sharp cut-off characteristic. In practice, however, no bandpass filter has this perfect cut-off. Several equivalent ideal bandwidths can be defined for such filters (see e.g. Bendat & Piersol 1971, p. 277) if the transfer function $H(f)$ is known. Here we shall assume that Δ corresponds to the so-called half-power bandwidth. That is,

$$\Delta = (f_2 - f_1)/f_m,$$

where f_1 and f_2 are defined by the equations

$$|H(f_1)|^2 = |H(f_2)|^2 = \tfrac{1}{2}|H(f_m)|^2.$$

We shall now adopt this definition and show that it is adequate for our purposes here. Other definitions of Δ make no essential difference.

Figure 2 shows a plot of $\hat{n}/\hat{n}_p$ versus $\hat{l}$ for white noise from a commercial random-noise generator (VEB Schwingungstechnik Akustik, type NRG 201) filtered by a Krohnhite filter (model 3202) at three midband frequencies of 500, 1000 and 2500 Hz. The curve is symmetrical with respect to $\hat{l} = 0$ as the data for $f_m = 1000$ Hz explicitly show. The Rayleigh distribution (2.17) is found to be in excellent agreement with measurements. In figure 3 measured values of $\hat{n}_p/\hat{f}_m \Delta$ are plotted for several values of f_m and two values of Δ. For the present experiments, Δ was determined by measuring the response of the filter; for the data of Rao *et al.*, although the authors

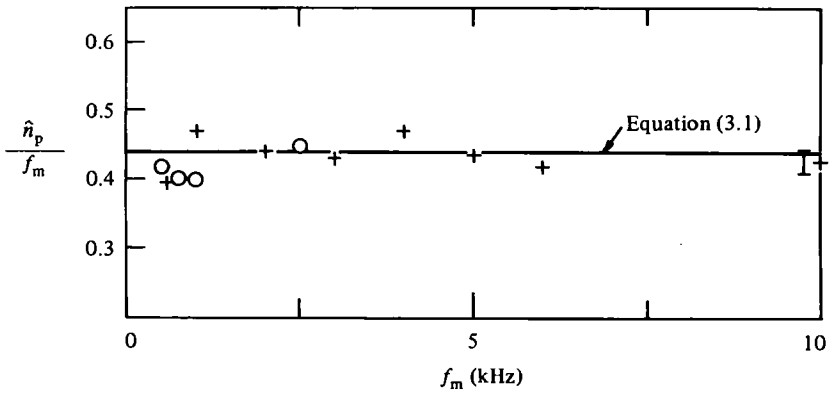

FIGURE 3. The peak pulse frequency in filtered white-noise signals as a function of midband frequency f_m and bandwidth Δ: ○, present data, $\Delta = 0.52$; +, Rao *et al.* (1971), $\Delta = 0.17$; ——, equation (3.1).

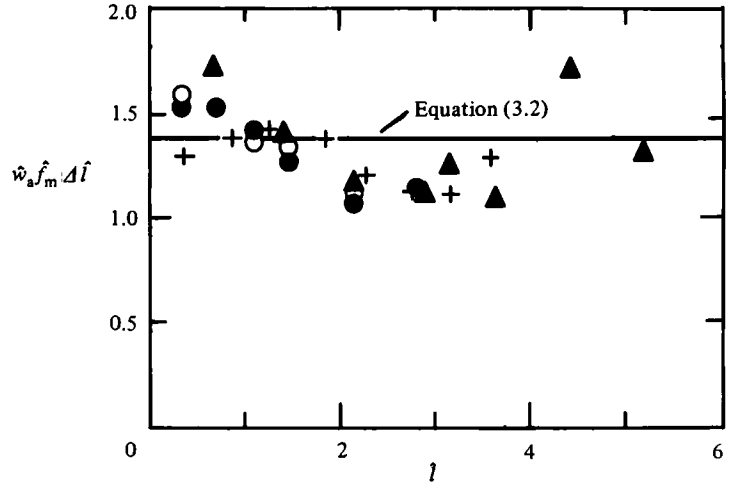

FIGURE 4. The mean pulse width in filtered white-noise signals as a function of f_m, Δ and $\hat{l}$: symbols as in figure 2; ——, equation (3.2).

did not explicitly mention the bandwidth of the filter they used, we have used a $\Delta = 0.17$ appropriate to their filter. It is seen that the ratio is a constant very close to the theoretical value given by (3.1). Figure 4 shows a plot of $\hat{W}_a \hat{f}_m \Delta \hat{l}$ for several bandpass-filtered Gaussian signals; although the uncertainty in measuring $\hat{W}_a$ for large $\hat{l}$ results in considerable scatter, it is clear that the trend is correctly predicted by the theory. Finally, figure 5 bears out (3.3) rather well.

In conclusion, we have demonstrated that the theoretical approach does indeed work in the expected manner.

3.2. *Non-white signals*

For later discussion, we consider here other Gaussian random processes whose spectral densities are not flat. Our concern will be the peak frequency $\hat{n}_p$, especially its asymptotic value $\hat{N}_p$ as $f_m \to \infty$ (see §1). Other parameters are given by (2.17)–(2.19).

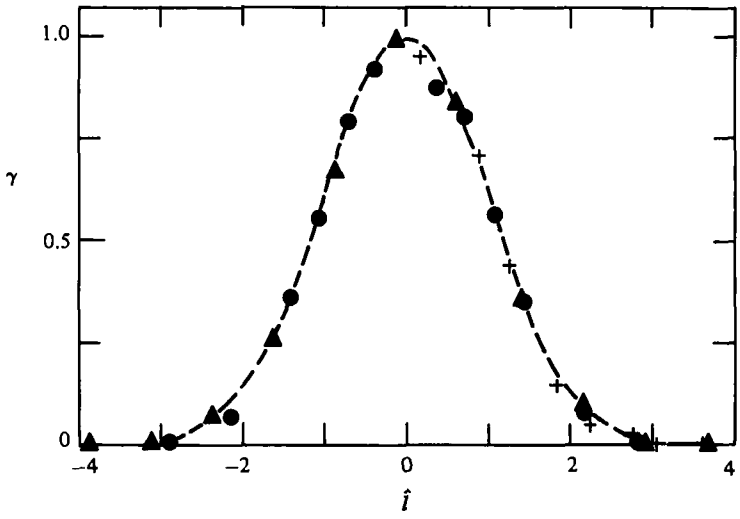

FIGURE 5. The (internal) intermittency factor γ as a function of the crossing level $\hat{l}$ for filtered white-noise signal: +, $f_m = 500$ Hz; ●, 1 kHz; △, 2.5 kHz; $\Delta = 0.52$ in all cases; ——, equation (2.18).

(i) $\phi(f) = cf^{-n}$, $n > 0$, and c independent of f. For this algebraic cut-off, it follows from (2.15) that

$$\hat{\xi} \sim f_m^2, \tag{3.4}$$

so that, from (2.16),

$$\hat{n}_p \sim f_m. \tag{3.5}$$

$\hat{N}_p$ is thus undefined.

(ii) $\phi(f) = c\,e^{-\alpha f}$, $\alpha > 0$. For this exponential roll-off, the corresponding results (spelled out in more detail here for future use) are

$$\hat{\xi} = \frac{2\pi}{\alpha^2}\left[1 - \frac{\zeta^2 e^{-\zeta}}{(1-e^{-\zeta})^2}\right], \quad \hat{n}_p = \frac{1.52}{\alpha}\left[1 - \frac{\zeta^2 e^{-\zeta}}{(1-e^{-\zeta})^2}\right]^{\frac{1}{2}}, \tag{3.6}$$

where $\zeta = \alpha f_m \Delta$. As $f_m \to \infty$, $\hat{\xi}$ and $\hat{n}_p$ tend to finite limits. It follows that

$$\hat{N}_p = \frac{1.52}{\alpha}. \tag{3.7}$$

(iii) As simple generalization of (ii) consider

$$\phi \sim f^r e^{-\beta f}.$$

The detailed expressions for $\hat{\xi}$ and $\hat{n}_p$ are complicated, but it not hard to show that

$$\hat{N}_p = 1.52(2r+1)^{\frac{1}{2}}/\beta. \tag{3.8}$$

(iv) As another generalization of (ii) consider

$$\phi = \sum_{n=1}^{\infty} a_r e^{-\beta_r f}, \quad \beta_r > \beta_{r-1};$$

it is easy to show that

$$\hat{N}_p = 1.52/\beta_1.$$

This follows from (ii) because, for larger f, other terms involving β_n ($n > 1$) becomes unimportant faster than the first term $a_1 e^{-\beta_1 f}$.

(v) Consider

$$\phi(f) = cf^r e^{-\beta^2 f^2}. \tag{3.9}$$

In this case, we have, for large f_m,

$$\xi \to 1 \quad \text{for all } r,$$

so that

$$\hat{N}_p = 1.52/\beta.$$

4. Bandpass-filtered turbulent signals

For reasons that will become clear in §4.2, it is useful to consider the data in turbulent shear flows separately from those in grid-generated turbulence.

4.1. *Turbulent shear flows*

Figure 6 shows the variation of $\hat{n}/\hat{n}_p$ as a function of the level $\hat{l}$ normalized by the root-mean-square of the bandpass-filtered signal. A variety of signals at different Reynolds numbers has been included here: those of Rao *et al.* were obtained by filtering at different midband frequencies the streamwise velocity fluctuation u in the inner layer; the present results are for u at $y/\delta = 0.3$ (at one midband frequency) and $y^+ \approx 5$ at several midband frequencies. In the present experiments, the velocity fluctuation u was obtained with a 5 μm diameter DISA hot wire operated on a DISA 55M01 constant-temperature anemometer. (Note: As no information is available on the root-mean-square value of the bandpass signals in the data of Rao *et al.*, the plots are adjusted such that $\hat{n}/\hat{n}_p = 1$ when $\hat{l} = 1$. For the present results, however, $\hat{l}$ was obtained from direct measurement.) Interestingly, these data have essentially the same behaviour as suggested by (2.17); further, this behaviour is common with turbulent signals in other shear flows (e.g. turbulent jets).

The mean width $\hat{W}_a$ of the pulses has also been measured in several flows. Figure 7 is a plot of $\hat{W}_a \hat{n}_p \hat{l}$ as a function of the Reynolds number R_λ in these flows. ($R_\lambda = u'\lambda/\nu$, where u' is the root-mean-square streamwise velocity, λ is the Taylor microscale and ν is the kinematic viscosity.) The relatively large scatter is not surprising considering the nature of these measurements, but it is clear that no apparent trend exists with R_λ, or with respect to the nature of the shear flow. In fact, the mean value of $\hat{W}_a \hat{n}_p \hat{l}$ data (0.55 ± 0.09) is within 10 % of the value of about 0.607 given by equation (2.19). Figure 8 shows that the γ versus $\hat{l}$ relation is described by (2.18) reasonably well.

What we have shown so far in this section is that the behaviours of the parameters $\hat{n}/\hat{n}_p$, $\hat{W}_a \hat{n}_p \hat{l}$ and γ can be explained quite well by our analytical procedure, which does not at all invoke the dynamics of turbulence. It is thus clear that if these quantities, normalized in the above manner, are to be indicators of internal intermittency at all, that property must come entirely through $\hat{l}$, the level of crossing (or, the threshold setting), the only one parameter on which depend the three quantities mentioned earlier. The picture is not complete, of course, until we can determine the precise way in which the peak pulse frequency $\hat{n}_p$, which we have used for normalization above, depends on the dynamics of the signal. Two crucial questions then are as follows. (*a*) What is the relation between the signal dynamics and the 'correct' threshold setting in internal intermittency measurements? (*b*) What aspects of signal dynamics are relevant to the determination of the scaling parameter $\hat{n}_p$? We shall relegate the discussion of (*a*) to §5, and consider (*b*) below.

For a Gaussian process, the factors influencing $\hat{n}_p$ are (see (2.14)–(2.16)) the filter bandwidth Δ, the midband frequency f_m and the spectral density $\phi(\omega)$. It may be

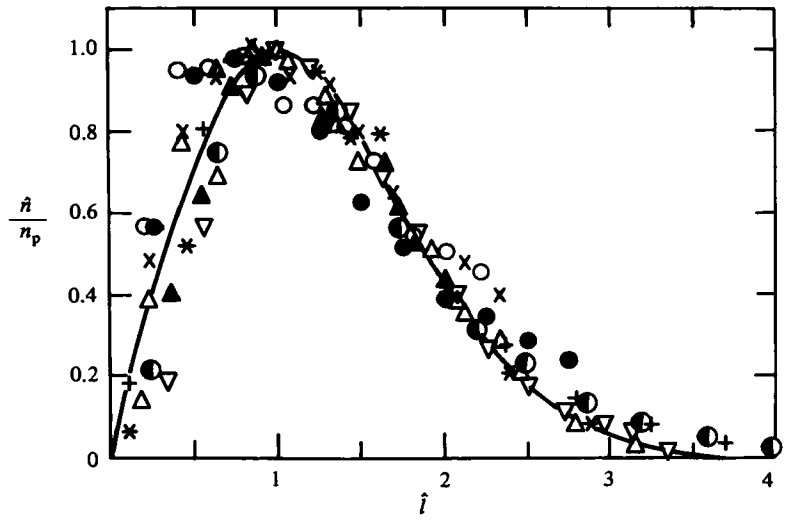

FIGURE 6. The pulse frequency $\hat{n}$ in filtered streamwise velocity fluctuations in turbulent boundary layers, as a function of the level of crossing $\hat{l}$. Present data: ▽, $y/\delta = 0.3$, $R_\theta = 7260$, $f_m = 5$ kHz; *, $f_m = 1.28$ kHz; △, 1.6 kHz; +, 2 kHz; ◐, 3.2 kHz. For the last four sets, $y^+ \approx 5$, $R_\theta = 1580$. Data of Rao *et al.* obtained in the inner layer, $R_\theta = 9450$: ▲, $f_m = 2$ kHz; △, 4 kHz; ●, 6 kHz; ×, 8 kHz; ○, 10 kHz. ——, equation (2.17).

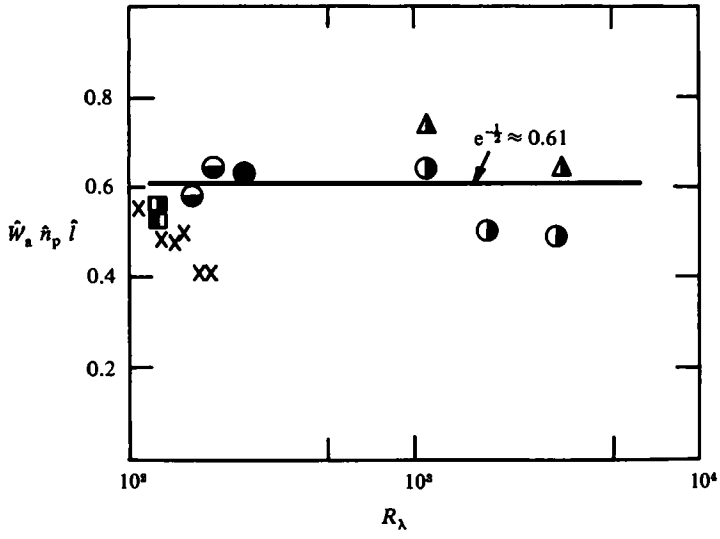

FIGURE 7. The mean pulse width in filtered turbulent signals on various shear flows, plotted as a function of the microscale Reynolds number. Present data for filtered u in turbulent boundary layers: ◨, $\hat{l} = 0.4$; ◧, $\hat{l} = 1.6$, both for $\hat{f}_m = 1.28$ kHz, $y^+ \approx 5$ and $R_\theta = 1580$; ○, $\hat{l} = 1$, $f_m = 5$ kHz, $y/\delta \approx 0.3$, $R_\theta = 7260$. Data of Badri Narayanan *et al.* for u in turbulent boundary layers: ×, $y/\delta \approx 0.4$, $R_\theta = 1900$–5500. Data of Antonia *et al.*: ◑, u; ◭, temperature fluctuation, both in the atmospheric surface layer; ◒, u, $y/\delta = 0.12$, $R_\theta = 5850$. Where unspecified, f_m is not accurately known. ——, equation (2.19).

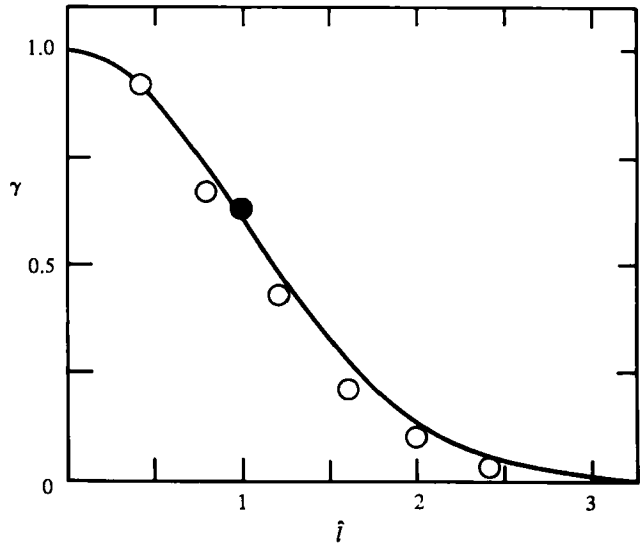

FIGURE 8. The (internal) intermittency factor γ as a function of the crossing level $\hat{l}$ for filtered u-signals in turbulent boundary layers: ●, $R_\theta = 1580$, $y^+ \approx 5$, $f_m = 1.28$ kHz; ○, $R_\theta = 7260$, $y/\delta = 0.3$, $f_m = 5$ kHz; ——, equation (2.18).

thought *a priori* that certain other factors (such as non-Gaussianity) would have to be included when dealing with turbulent signals. However, the success we have so far had with the theory suggests that it is worth evaluating $\hat{n}_p$ without considering these extra 'complications', and so we pragmatically take from measurements the spectral density $\phi(\omega)$ of the particular signal under question, and evaluate $\hat{n}_p$. If the $\hat{n}_p$ so evaluated (for given f_m and Δ) differs substantially from measurement, some of the features excluded at this stage from the theory may be inferred to be important. In the absence of any substantial disagreement, we should conclude that the important aspects of turbulence dynamics (only in so far it relates to $\hat{n}_p$!) somehow enter essentially through the spectral density, and that the other features like non-Gaussianity are not in themselves critical. (We should like to add, even if somewhat unnecessarily, that non-Gaussianity is of undoubted importance in many other aspects of internal intermittency, such as the flatness factor and the skewness. It also enters (via the choice of the most appropriate threshold setting) in the determination of $\hat{n}$ and $\hat{W}_a$; see §5.)

First, we show in figure 9 the $\hat{n}_p$ measurements in boundary layers; other flows are known to be no different. As discussed in §1, the peak pulse frequency $\hat{n}_p$ initially increases with increasing midband frequency, and appears to settle down to a constant value in the far-dissipation region. This is a typical result; more data can be found in Rao *et al.* (1971). The nearly linear initial rise of $\hat{n}_p$ with f_m is not surprising in view of the relatively flat spectral content in that frequency range (see (3.1)), but an interesting feature is that $\hat{n}_p$ settles down to a constant fraction of the Kolmogorov frequency f_η, for $f_m/f_\eta \gtrsim 0.5$. Rao *et al.* interpreted this constancy of $\hat{n}_p$ with f_m for large f_m as follows. Whenever a wideband signal is passed through a narrow-band-pass-filter of bandwidth Δf_m, the output of the filter is an amplitude-modulated signal, with the characteristic modulation frequency proportional to Δf_m itself. Since the resultant modulation is what one identifies with pulses, it is clear that the pulse frequency $\hat{n}_p$ should be proportional to Δf_m, or proportional for f_m itself since Δ is a constant). In general, therefore, $\hat{n}_p \propto f_m$, a result that we have shown, both

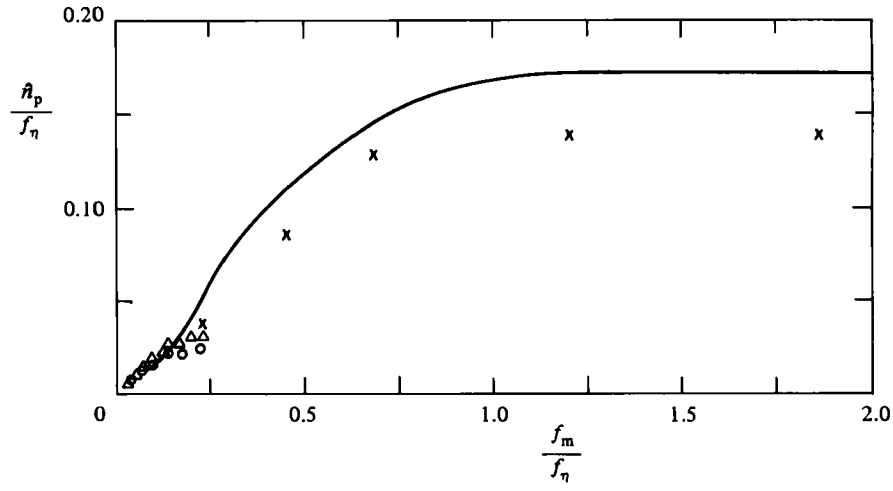

FIGURE 9. The (normalized) peak pulse frequency as a function of the midband frequency f_m; data for turbulent boundary layers: ○, Badri Narayanan *et al.* (1974), $y/\delta = 0.4$, $R_\theta = 3000$; △, Antonia *et al.* (1976), $y/\delta = 0.12$, $R_\theta = 5850$; ×, present, $y/\delta = 0.3$, $R_\theta = 1580$; ——, theoretical calculations using (4.1). f_η is the Kolmogorov frequency given by $U/2\pi\eta$, η being the Kolmogorov microscale.

analytically and experimentally, to be true for white noise. (This is true also for a Markov process whose spectral density asymptotes to a power-law roll-off; see (3.1) and (3.5).) The fact that $\hat{n}_p$ settles down to a constant was thus attributed by Rao *et al.* to genuine internal intermittency.

With this in background, it is now appropriate to consider what *a priori* considerations in the theory would have suggested that $\hat{n}_p \to$ constant as $f_m \to \infty$. We recall from section 3.2 that the only spectral shapes for which $\hat{n}_p \to$ constant as $f_m \to \infty$ are $\phi \sim f^r e^{-\alpha f}$, $\phi \sim e^{-\alpha f}$ and $\phi \sim f^r e^{-\beta^2 f^2}$. Within the framework of the theory, we thus conclude that the approach of $\hat{n}_p$ to a constant implies that the roll-off of $\phi(f)$ should be faster than algebraic.† It was pointed out several years ago by Kraichnan (1967) than a faster-than-algebraic decay in the far-dissipation range implies strong intermittency, no matter what the Reynolds number. Kraichnan's point was simply that, given a stronger-than-algebraic decay of the spectral density, the existence of the mean square of all velocity derivatives implies that the spectral density at any fixed wavenumber in the relevant wavenumber range comes from a few exceptional regions only – a typical attribute of fine-scale intermittency. More recently, Frisch & Morf (1981) have also reached essentially the same conclusion, based on a more quantitative analysis in the complex domain of the nonlinear Langevin equation.

To carry further the notion that the internal intermittency and the stronger-than-algebraic decay in the far-dissipation range are tied together, we shall now calculate the actual numbers in the $(\hat{n}_p, f_m)$-relation shown in figure 9. Obviously, the notion derives stronger support if we can also quantitatively predict the observed $(\hat{n}_p, f_m)$-relation.

A brief digression is necessary. Stewart & Townsend (1951) have shown that in grid turbulence the measured one-dimensional spectral density preserves its shape in the dissipation range when normalized on the Kolmogorov velocity scale and lengthscale.

† In fact, we can be somewhat more specific and exclude the case $\phi \sim f^n e^{-\alpha f}$ on the grounds that the results become meaningless for $n \lesssim -0.5$ (see (3.8)), and it is in practice not possible to fit a curve $f^n e^{-\alpha f}$ to the measured spectral density of $n \gtrsim -0.5$.

The conclusion empirically holds true for shear flows also. We have examined in the Appendix all the high-frequency spectral data in boundary layers as well as grid turbulence, and borrow from there the result that the self-preserving shape is satisfactorily described by the (empirical) expressions

$$\left.\begin{aligned} \frac{\phi}{v^2\eta} &\sim \exp\left(-12.7\frac{f}{f_\eta}\right) \quad \text{for } 0.1 \lesssim \frac{f}{f_\eta} \lesssim 0.5, \\ &\sim \exp\left(-8.8\frac{f}{f_\eta}\right) \quad \text{for } 0.5 \lesssim \frac{f}{f_\eta} \lesssim 1.5, \end{aligned}\right\} \tag{4.1}$$

where v is the Kolmogorov velocity.

We may now complete the $\hat{n}_p$ calculations in the range $0.1 \lesssim f/f_m \lesssim 1.5$ using (3.6).† It is seen from figure 9 that the data from all the sources are in reasonable agreement with this theoretical calculation. We shall return to a discussion of this result in §5. (More recently, Antonia *et al.* (private communication) have produced $\hat{n}_p$ data which tend to asymptote at around $f/f_\eta \approx 1.0$ before sharply increasing again. Spectral measurements show that noise effects become important around f_η.)

4.2. *Grid turbulence*

Consider the Kuo–Corrsin data of 1971. They measure both the intermittency factor γ and the mean width $\hat{W}_a$ of the high-frequency pulses. In determining these quantities, the threshold (equivalent to our $\hat{l}$) was set to different values for each set of $(\hat{W}_a, \gamma)$-measurements, but the precise value of $\hat{l}$, one of the important parameters in our theory, were not recorded. Thus the best we can do is to evaluate it from our theory using one of the measured quantities $\hat{W}_a$ or γ, and predict the other. If the prediction is reasonable, we conclude that the data are consistent with the theory. Clearly the comparison between theory and experiment is not as complete as in the case of boundary layers; this, of course, is the reason for considering grid-turbulence data separately.

Two possibilities arise. One of them is to assume that the intermittency factor γ is given, and evaluate $\hat{l}$ from (2.11), which gives

$$\hat{l} = (-2\ln\gamma)^{\frac{1}{2}}. \tag{4.2}$$

Using this $\hat{l}$, and the theoretical prediction of $\hat{n}_p$ from (3.6) and (4.1), we can evaluate from (2.12) the mean width $\hat{W}_a$ of the active regions. The other possibility is to assume $\hat{W}_a$ as given, and evaluate $\hat{l}$ from (2.12) using the theoretically determined $\hat{n}_p$; we can then predict γ from (2.11). We have done both.

Figures 10(*a*, *b*) show the measured values of the intermittency factor γ and the width $\hat{W}_a$ of the pulses. From these two, one can compute the pulse frequency $\hat{n}\,(=\gamma/\hat{W}_a)$, also plotted in figure 10(*c*). The unbroken lines in figures 10(*b*, *c*) are the theoretical calculations for $\hat{W}_a$ and $\hat{n}$, obtaining $\hat{l}$ from the measured γ; that in figure 10(*a*) represents the actual smoothing we have used for γ in getting $\hat{l}$ from (4.2). The dashed line in figures 10(*a*, *c*) are the theoretical calculations for γ and $\hat{n}$, with $\hat{l}$ obtained from the measured $\hat{W}_a$, which itself is represented by the dashed line in figure 10(*b*). It is seen that the agreement between the experiment and either set of calculations is only qualitatively correct. We believe that part of the reason for no better quantitative agreement rests with the limitations of the procedure we have been forced to adopt, namely to assume that one or the other of the two measured parameters is precise. If we assume, for example, that neither of the measured

† It is necessary to patch smoothly around $f_m/f_\eta \approx 0.5$ the results from the two expressions (4.1); no formal matching is possible.

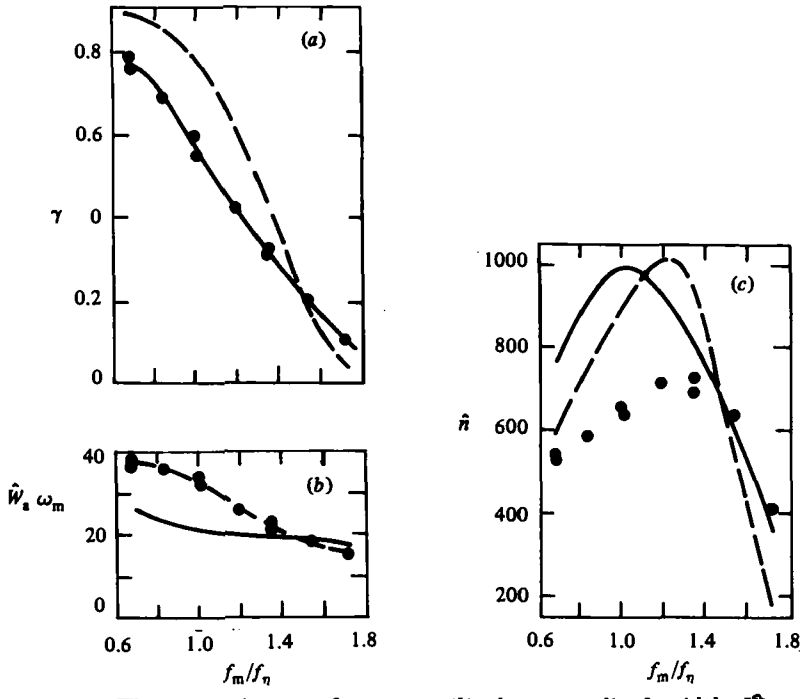

FIGURE 10. (*a*) The intermittency factor, γ; (*b*) the normalized width $\hat{W}_a\omega_m$ of the pulses ($\omega_m = 2\pi f_m$); (*c*) the pulse frequency $\hat{n}$ ($\equiv \gamma/\hat{W}_a$) for grid turbulence. Data from Kuo & Corrsin (1971), $R_\lambda = 110, f_m = 5900$ Hz. —— and -- are theoretical predictions explained in the text.

parameters is correct to better than 10%, we can in fact produce a better overall agreement by 'splitting the difference' between γ and $\hat{W}_a$. Our objective is not to suggest that the measurements are inaccurate, but to point out that realistic uncertainties could affect the quality of our comparison in figure 10.

Finally, we have formed the product $\hat{W}_a\,\hat{n}_p\,\hat{l}$ for the Kuo–Corrsin data at the three Reynolds numbers of their measurement; the objective is to compare this product with prediction from (2.12). In forming this product, $\hat{W}_a$ was taken from measurement directly and $\hat{l}$ was obtained from measured γ using (4.2). The peak pulse frequency $\hat{n}_p$ was obtained in two steps, first by getting $\hat{n}$ from measurement ($\equiv \gamma/\hat{W}_a$) and then converting it to $\hat{n}_p$ using the theoretical ratio $\hat{n}/\hat{n}_p$; since the midband frequency f_m was set equal to f_η in these measurements, $\hat{n}/\hat{n}_p \approx 1$ (see figure 9). Thus we took $\hat{n}_p = \hat{n} = \gamma/\hat{W}_a$. The product $\hat{W}_a\,\hat{n}_p\,\hat{l}$ given in table 1 shows that the agreement with the theory is not unreasonable.

In sum, we believe that the grid-turbulence data are also not inconsistent with the theory.

5. Discussions and conclusions

It is useful to summarize our results here. We have shown in §§3 and 4 that

$$\hat{n}/\hat{n}_p = f_1(\hat{l}), \quad \hat{W}_a\,\hat{n}_p = f_2(\hat{l}), \quad \gamma = f_3(\hat{l}),$$

where f_1, f_2 and f_3 are known functions only of the threshold setting $\hat{l}$. Thus the two basic characteristics of an intermittent signal, namely $\hat{n}$ and $\hat{W}_a$ (note: $\gamma = \hat{n}\hat{W}_a$) are dependent only on $\hat{l}$ and the characteristic pulse frequency $\hat{n}_p$. All the dynamical characteristics of the signal, as well as the filter settings (such as the bandwidth and the midband frequency), enter only indirectly in so far as they determine $\hat{l}$ and $\hat{n}_p$.

	$\hat{W}_a \hat{n}_p \hat{l}$	
R_λ	Experiment	Theory
50	0.46	0.605
73	0.57	
110	0.61	

TABLE 1. The product $\hat{W}_a \hat{n}_p \hat{l}$ from the grid-turbulence measurements of Kuo & Corrsin

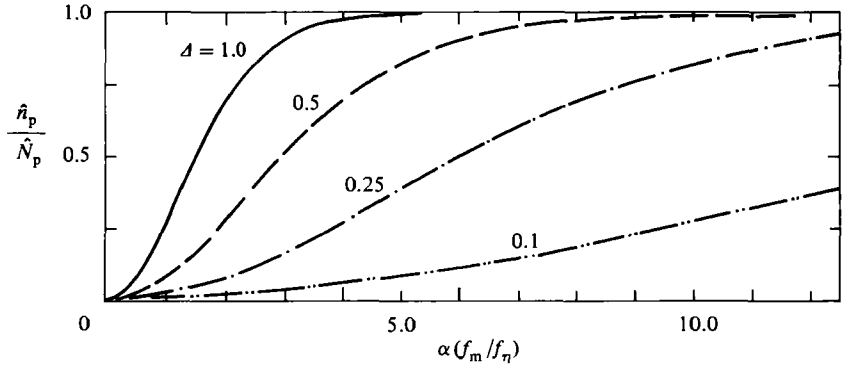

FIGURE 11. The effect of midband frequency f_m and the filter bandwidth Δ on the peak pulse frequency $\hat{n}_p$.

Let us first consider $\hat{n}_p$. The effect of filter characteristics on $\hat{n}_p$ can be illustrated by taking the spectral density ϕ to be given by $\exp\{-a(f/f_\eta)\}$; when f/f_η is not too small, this is typically the form we discussed in §4. Figure 11 shows the variation of the peak pulse frequency $\hat{n}_p$ as a function of f_m and Δ. Notice that, the larger the bandwidth, the earlier in f_m is the aymptotic state reached. (This is to be expected because larger values of the bandwidth imply that the tail end of the spectrum representing the intermittent region is incorporated for lower settings of the filter midband frequency.) It is clear that, even if one measures the peak pulse frequency for the same signal at the same f_m, one can come up with different values for $\hat{n}_p$ depending on the filter bandwidth. On the other hand, the asymptotic value $\hat{N}_p$ of $\hat{n}_p$ is independent of the filter bandwidth (see (3.7)). We conclude that $\hat{N}_p$ is a very important characteristic (because it is determined completely by the signal dynamics in a way we can determine; see below) of internal intermittency in the far-dissipation region.

Regarding the dynamical aspects of the signal that go into determining $\hat{n}_p$, we have shown that $\hat{n}_p$ measurements in the far-dissipation region can be explained correctly, provided the spectral density in the far-dissipation range is assumed to have a stronger-than-algebraic roll-off. The question that naturally arises is whether this requirement on the roll-off characteristics of ϕ is merely an artifact of our having persisted with Gaussianity assumption for the filtered version of $u(t)$,† knowing full

† We would like to emphasize that our theory does not assume that $u(t)$ is Gaussian, but only its narrow-bandpass version is. Narrow-bandpass filtering introduces considerable smoothing, and a smoothing of a non-normal stochastic process makes it tend towards normality. Probability density measurements of narrow-bandpass-filtered turbulent-velocity signals actually show that the departures from Gaussianity are significant only towards the tails; these departures, while being *crucial* for the flatness factor and the skewness (for example), do not seem to be important in the context of the intermittency measures *we have considered*.

well that it cannot be completely correct. We do not have a conclusive answer, because for no other probability distribution can the results be made as explicit as has been possible here. There exist several pointers, however. First, Kraichnan's conclusion that internal intermittency implies a stronger-than-algebraic spectral roll-off did not have to use normality assumption in any way. This suggests to us that the complementary conclusion, that only the stronger-than-algebraic spectral roll-off will reproduce the observed $(\hat{n}_p f_m)$-relation, may also be independent of the normality assumption. Furthermore, our limited experimentation suggests that a small perturbation on a Gaussian process does not matter much for the internal intermittency measures discussed here. Together, they lead us to believe that the assumption of Gaussianity in our theory is probably only incidental, and simply the most convenient; it follows that the stronger-than-algebraic decay of ϕ in the far-dissipation range may be a genuine characteristic of internal intermittency. Perhaps, this is characteristic of all intermittent nonlinear processes. The work of Frisch & Morf (1981) has gone farthest in elucidating this point. These authors have shown, with particular reference to the nonlinear Langevin equation, that the exponential nature of the spectral density in the far-dissipation region can be related to the singularities of the equation in the complex plane. Whether the Navier–Stokes equations are singular in the complex plane is, however, an open question.

If it is true that $\hat{n}_p$ can also be considered a known quantity, it follows that the only parameter that sets apart different signals as regards their intermittency characteristics is the threshold setting l. The most important question in internal intermittency measurements is therefore: 'What is the correct threshold setting that one should choose?' A complete theory should of course reveal how l must depend on the dynamical characteristics of the signal itself (and the filter settings); the present theory is incapable of providing an answer to this question, precisely because the dynamical considerations we have ignored all along will certainly become important here. Several considerations go into the determination of the correct threshold level, but the most important step is clearly subjective.† Therein lies the weakness of all internal intermittency measurements involving the frequency of pulses, intermittency factor and the pulse width.

In spite of this subjectivity, it is useful to take guidance from typical measurements and discuss how the 'correct' values of the threshold l may depend on the dynamical characteristics of the signal. Figure 12 shows the empirically determined threshold for filtered turbulence signals. Assuming that the subjective judgement that goes into determining these data is correct, the figure shows that l increases with increasing midband frequency (i.e. the signal becomes more and more intermittent at smaller and smaller scales). For white noise, on the other hand, l does not depend on f_m, and γ is therefore independent of f_m.

Because of the subtle influences that various factors have on internal intermittency measurements, and because of the extreme sensitivity of the results on the threshold setting, it is not surprising that different authors have arrived at different values for the several measures of intermittency, often with conflicting conclusions (see §1).

† Briefly, one generates an indicator function $I(t)$ that is a random square wave such that $I(t) = 1$ whenever the signal exceeds the chosen threshold, and zero otherwise. One then compares $I(t)$ with the filtered signal to determine whether the threshold chosen is 'correct'. This last step is crucial but subjective. For the correct setting $\gamma = I(t)$. This technique, originally used in the outer-layer intermittency measurements in free shear flows, is due to Townsend (1948). Other sophistications introduced later (see e.g. Kuo & Corrsin 1971; Hedley & Keffer 1974) do not eliminate the need for the final subjective comparison of $I(t)$ with the original signal.

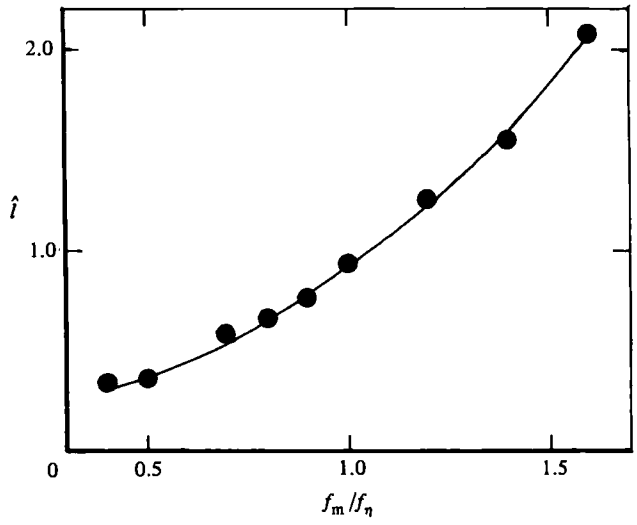

FIGURE 12. The experimentally determined threshold setting as a function of the midband filter frequency. Data for u in a turbulent boundary layer, $R_\theta = 1580$, $y/\delta = 0.3$.

What we have shown is that, if all factors are properly taken into account, the seemingly confusing picture becomes quite clear. Part of the contribution of this paper is in sorting out this confusion by way of determining the precise roles of each of the parameters entering the problem.

I cannot exaggerate the impact on this work of a brief conversation I had some eight years ago with Professor R. Narasimha. I should also like to thank Professor R. A. Antonia and Dr D. Britz for their most penetrating comments on an earlier draft. Thanks are due to Dr H. Oertel of DFVLR, Göttingen, for the hospitality extended at his institute while the manuscript was being completed. During part of my stay at DFVLR, I was awarded a fellowship from the Alexander von Humboldt foundation.

Appendix

Figure 13 shows some high-frequency spectral data of u in turbulent boundary layers; also plotted are data for a high-Reynolds-number ($Re = 500000$) pipe flow of Laufer (1954). It is clear that a reasonable degree of self-preservation exists in the Kolmogorov variables (although the details of Kolmogorov's arguments cannot be expected to hold in shear flows).

Except for our own data in figure 13, the other two sources of data are quite old. Relatively more recently, Comte-Bellot & Corrsin (1971) have obtained high-frequency spectral data in grid turbulence for two Reynolds numbers and at several locations behind the grid. We have plotted their data in figure 14, again normalizing by the Kolmogorov scales. They too confirm an excellent tendency towards self-preservation; note that the energy scale spans about eight decades in this region. Except for the last two points of Klebanoff's data, figures 13 and 14 are quite comparable where they overlap.

To determine the best exponential fit for ϕ, we have plotted in figure 15 data from both figures in the form $\ln(\phi/v^2\eta)$ versus f/f_η. We can see that the two expressions given in (4.1) fit the data well in the respective ranges.

High-frequency spectral data are difficult to obtain accurately, and are plagued

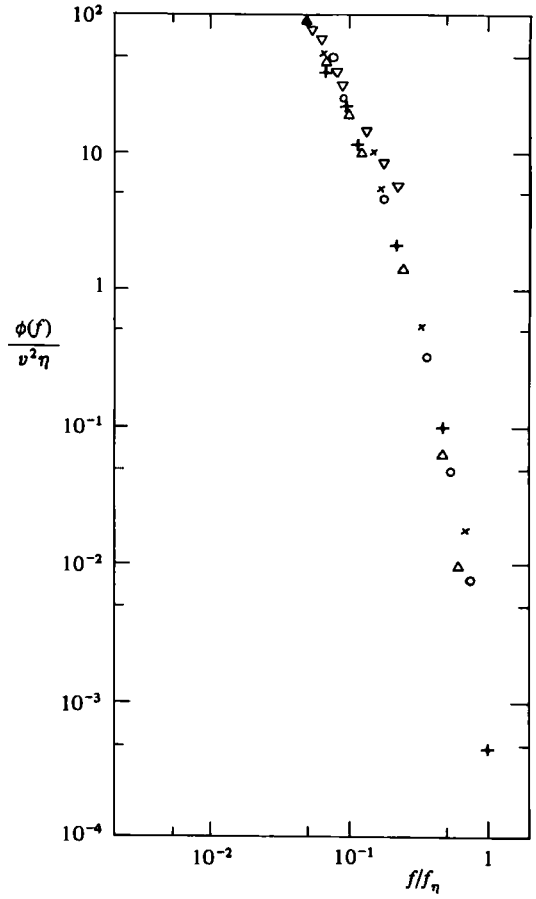

FIGURE 13. Self-preservation of the high-frequency end of the spectral density in shear-flow turbulence. Boundary-layer data from Klebanoff (1955). $R_\delta = 75000$: ○, $y/\delta = 0.05$; △, 0.20; ×, 0.58. ▽, pipe-flow data from Laufer (1954), $R_a = 500000$, $y/a = 0.074$, where a is the pipe radius. ×, present data, $R_\theta = 1580$, $y/\delta \approx 0.3$.

by uncertainties such as noise and effects of the finite length of the hot wire. It is nevertheless heartening to note that all the data agree within reason. Most sets of data in figures 13 and 14 were corrected for electronic noise and 'empty tunnel disturbances', but none was corrected for the finite-length effects of the hot wire. Comte-Bellot & Corrsin (1971) note that this last correction was within the measurement scatter.

The precise value of the coefficient a in $\phi \sim \exp\{-a(f/f_\eta)$ corresponding to the second expression in (4.1) determines in our theory the asymptotic value $\hat{N}_p$ of $\hat{n}_p$. A 20% change, for example, in the value of a (should such a change be necessitated by improved data that may be acquired in future with more sophisticated instrumentation) will produce a 20% variation in $\hat{N}_p$, but this does not affect our conclusions. In fact, a 20% larger a will produce a better fit to our own $\hat{n}_p$ data in figure 9, as well as to the Kuo–Corrsin data in figures 10.

The observed universality of the spectrum when plotted in the Kolmogorov variables suggests (see (2.7) and (2.8)) that $\hat{n}_p/f_\eta$ must be a unique function of f_m/f_η for f_m/f_η not too small. That, of course, is why we plotted data in figure 9 the way we have. Considering the difficulty in making the $\hat{n}_p$ measurements, figure 9 can be considered to support the contention.

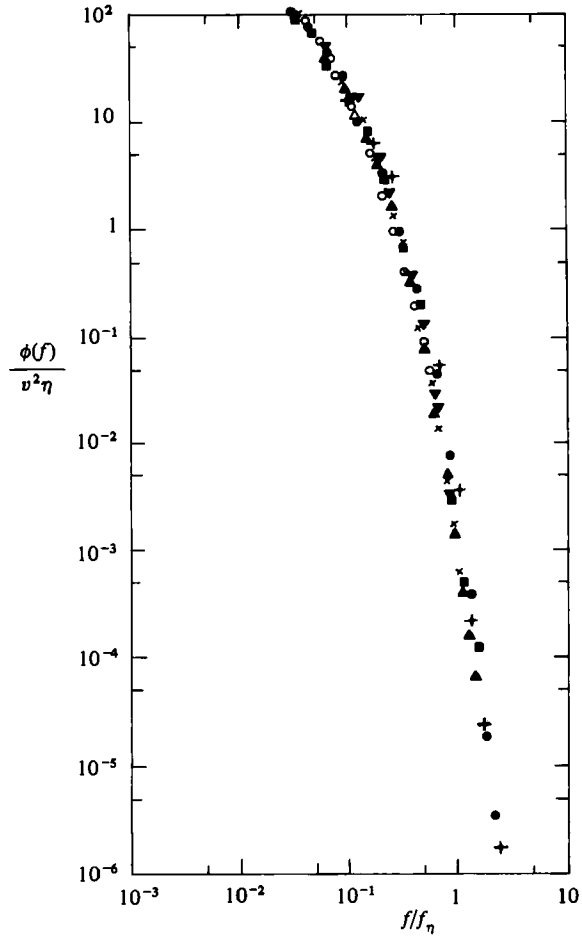

FIGURE 14. Self-preservation of the high-frequency end of the spectral density of the longitudinal component of velocity in grid turbulence. Data from Comte-Bellot & Corrsin (1971). $UM/\nu = 3.39 \times 10^4$; ○, $x/M = 42$; ×, 98; ▲, 171. $UM/\nu = 1.69 \times 10^4$: ▼, $x/M = 45$; ■, 120; +, 210; ●, 385. v is the Kolmogorov velocity scale and f_η is the Kolmogorov frequency.

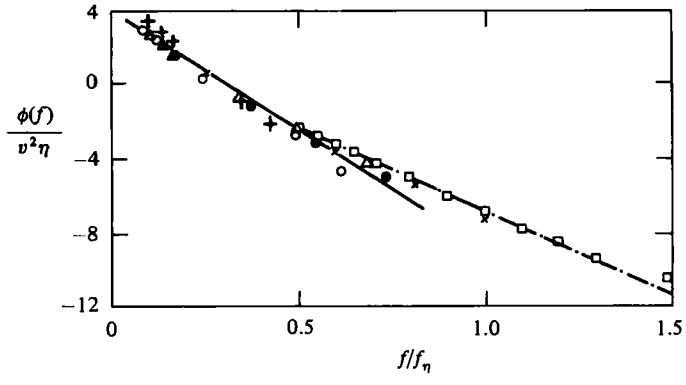

FIGURE 15. The exponential fits to the tail-end of the Kolmogorov-normalized spectral data. □ represents the mean of the grid-turbulence data of figure 14; other symbols as in figure 13.

REFERENCES

ANTONIA, R. A., DANH, H. Q. & PRABHU, A. 1976 *Phys. Fluids* **19**, 1680.

BADRI NARAYANAN, M. A., NARASIMHA, R. & RAO, K. N. 1971 In *Proc. 4th Australasian Conf. on Hydraulics and Fluid Mechanics, Monash University, Melbourne, Australia*, p. 73.

BADRI NARAYANAN, M. A., RAJAGOPALAN, S. & NARASIMHA, R. 1974 *Rep.* 74 FM 15, *Dept Aero. Engng, Indian Institute of Science, Bangalore.*

BADRI NARAYANAN, M. A., RAJAGOPALAN, S. & NARASIMHA, R. 1977 *J. Fluid Mech.* **80**, 237.

BATCHELOR, G. K. & TOWNSEND, A. A. 1949 *Proc. R. Soc. Lond.* A **199**, 238.

BENDAT, J. S. & PIERSOL, A. G. 1971 *Random Data: Analysis and Measurement Procedures.* Wiley.

BRACEWELL, R. 1965 *The Fourier Transform and Its Applications.* McGraw-Hill.

BRACHET, M. E., MEIRON, D. I., ORSZAG, S. A., NICKEL, B. G., MORF, R. H. & FRISCH, U. 1983 *J. Fluid Mech.* **130**, 411.

COMTE-BELLOT, G. & CORRSIN, S. 1971 *J. Fluid Mech.* **48**, 273.

CORRSIN, S. 1962 *Phys. Fluids* **5**, 1301.

CRAMER, H. & LEADBETTER, M. R. 1967 *Stationary and Related Stochastic Processes.* Wiley.

FRISCH, U. & MORF, R. 1981 *Phys. Rev.* A **23**, 2673.

FRISCH, U., SULEM, P.-L. & NELKIN, M. 1978 *J. Fluid Mech.* **87**, 719.

GRANT, H. L., STEWART, R. W. & MOILLIET, A. 1962 *J. Fluid Mech.* **12**, 241.

HEDLEY, T. B. & KEFFER, J. F. 1974 *J. Fluid Mech.* **64**, 625.

KENNEDY, D. A. & CORRSIN, S. 1961 *J. Fluid Mech.* **10**, 366.

KLEBANOFF, P. 1955 *NACA Tech. Rep.* 1247.

KOLMOGOROV, A. N. 1941 *C.R. Acad. Sci. USSR* **30**, 301.

KOLMOGOROV, A. N. 1962 *J. Fluid Mech.* **13**, 81.

KRAICHNAN, R. H. 1967 *Phys. Fluids* **10**, 2080.

KRAICHNAN, R. H. 1974 *J. Fluid Mech.* **62**, 305.

KUO, A. Y. S. & CORRSIN, S. 1971 *J. Fluid Mech.* **50**, 285.

KUO, A. Y. S. & CORRSIN, S. 1972 *J. Fluid Mech.* **56**, 447.

LAUFER, J. 1954 *NACA Tech. Rep.* 1174.

MANDELBROT, B. 1976 In *Turbulence and Navier–Stokes Equations* (ed. R. Temam). Lecture Notes in Maths, vol. 565, p. 121. Springer.

NOVIKOV, E. A. & STEWART, R. W. 1964 *Izv. Acad. Sci. USSR, Geophys. Ser.* **3**, 408.

RAO, K. N., NARASIMHA, R. & BADRI NARAYANAN, M. A. 1971 *J. Fluid Mech.* **48**, 339.

RUELLE, D. 1980 *Math. Int.* **2**, 126.

SAFFMAN, P. G. 1968 Lectures in homogeneous turbulence. In *Topics in Nonlinear Physics* (ed. N. Zabusky), p. 485. Springer.

SANDBORN, V. A. 1959 *J. Fluid Mech.* **6**, 211.

SIGGIA, E. 1981 *J. Fluid Mech.* **107**, 375.

SREENIVASAN, K. R. 1984 *Phys. Fluids* **27**, 1048.

STEWART, R. W. & TOWNSEND, A. A. 1951 *Phil. Trans. R. Soc. Lond.* A **243**, 359.

TENNEKES, H. 1968 *Phys. Fluids* **11**, 669.

TOWNSEND, A. A. 1948 *Austral. J. Sci. Res.* A **1**, 161.

TOWNSEND, A. A. 1951 *Proc. R. Soc. Lond.* A **208**, 534.

UEDA, H. & HINZE, J. O. 1975 *J. Fluid Mech.* **67**, 137.

VAN ATTA, C. W. & ANTONIA, R. A. 1980 *Phys. Fluids* **23**, 252.

YAGLOM, A. M. 1966 *Sov. Phys. Dokl.* **11**, 26.